

# ROBUST TIME-DOMAIN MIGRATION VELOCITY ANALYSIS METHODS FOR INITIAL-MODEL BUILDING IN A FULL WAVEFORM TOMOGRAPHY WORKFLOW

*H. B. Santos, J. Schleicher, A. Novais, A. Kurzmann, and T. Bohlen*

**email:** *hbuenos@gmail.com, js@ime.unicamp.br*

**keywords:** *Migration velocity analysis, time-to-depth conversion, acoustic full waveform tomography, velocity model building*

## ABSTRACT

*Full-waveform tomography (FWT) is notorious for its strong dependence on the initial model. We present a workflow for the construction of initial velocity-models for FWT methods consisting of automatic time-migration velocity analysis by means of double multi-stack migration, followed by time-to-depth conversion by image-ray wavefront propagation. Evaluation of the converted velocity model as an initial velocity model in an acoustic FWT process indicates the potential of using a combination of these methods to achieve a fully automatic tool for initial-model building in a FWT workflow. Our tests on a modified version of the Marmousi-2 model have shown that correct background velocity information can be successfully extracted from automatic time-domain migration velocity analysis even in media where time-migration cannot provide satisfactory seismic images.*

## INTRODUCTION

In 1984, Tarantola presented the basic idea of acoustic full waveform inversion (FWI) as a local optimization method that aims to minimize the least-squares misfit between observed and modeled seismograms. In other words, the aim of FWI is to find a subsurface model which explains the recorded seismic data (Symes, 2008). Toward the end of the 80's, Mora (1987a,b) and Tarantola (1986) extended the theory to the elastic case. Shortly after, Pratt and Worthington (1990) and Pratt (1990) introduced the frequency-domain version of full waveform inversion. While its high computational cost retarded its adoption for almost two decades, advance of computing technology allowed to develop multiscale inversion, which became an area of very busy and active research, and it provided a hierarchical framework for robust inversion (Yang et al., 2015).

FWI proved to be an efficient tool for the determination of high-resolution details in multi-parameter models of complex subsurface structures, and it has been applied in different geophysical problem scales, ranging from ultrasonic data (Pratt, 1999) to seismological imaging (Fichtner et al., 2009).

Being a highly nonlinear problem, FWI techniques face other drawbacks than their elevated computational cost. They are notorious for depending strongly on the choice of a good starting model for convergence at a geologically meaningful result. Analysing this dependence, Mora (1989) recognized that FWI has a migration component and a tomographic component. To ensure convergence of the tomographic component, a possible strategy is to start the inversion processing from the low frequencies, but this does not avoid the need of accurate initial velocity models (Biondi and Almomin, 2014).

For this reason, quite some effort has been made to come up with initial models for FWI. Traveltime tomography, Laplace-domain inversion and migration-based velocity analysis (MVA) are some examples of seismic techniques that have been investigated for this purpose (Prioux et al., 2012).

In this paper, we investigate another possible strategy with potential to help the construction of initial velocity models for full-waveform tomography (FWT). We apply the double multi-stack technique of Schleicher and Costa (2009) to perform a time-domain MVA. This is a fully automatic tool that is useful to obtain a migration velocity model and its corresponding time migrated image in a computationally effective way. We then convert the time-migration velocity model to the depth domain by means of the time-to-depth conversion strategy based on image-wavefront propagation (Valente, 2013; Valente et al., 2014; Santos et al., 2015). We evaluate the converted velocity model as an initial velocity model in an acoustic FWT process (Kurzmann et al., 2013). For comparison, we carry out the same FWT using three other starting models.

## METHODOLOGY

In this section, we give a brief summary of the methods we use to compose our workflow for initial-velocity model building and FWT.

### MVA by double multi-stack migration

The workflow starts with the double multipath time migration-velocity analysis of Schleicher and Costa (2009). This MVA technique is based on the multipath-summation imaging process of Landa et al. (2006). The fundamental idea of the latter is to stack the migration results for “all possible” velocities, or at least as much models as practically reasonable. Since only “good” models yield flat events in common-image gathers, these will prevail in the overall stacked image, which thus will show the geologic structure without the need for a migration-velocity model. Below, we will refer to this technique as multi-stack migration.

The multi-stack time-migration operator can be written as

$$V_w(\mathbf{x}) = \int d\alpha w(\mathbf{x}, \alpha) \int d\xi \int dt U(t, \xi) \delta(t - t_d(\xi, \mathbf{x}; \alpha)), \quad (1)$$

where  $V_w$  is the resulting time-migrated image at an image point with coordinates  $\mathbf{x} = (x, \tau)$ ,  $x$  being the lateral distance,  $\tau$  vertical time,  $U(t, \xi)$  a seismic trace at coordinate  $\xi$  in the seismic data,  $t_d(\xi, \mathbf{x}; \alpha)$  is a stacking surfaces corresponding to a set of possible velocity models that are parameterized using variable  $\alpha$  and  $w(\mathbf{x}, \alpha)$  is a weight function, which serves to attenuate contributions from unlikely trajectories and emphasize contributions from trajectories close to the optimal. In the application of Schleicher and Costa (2009),  $\alpha$  directly represented the time-migration velocity and the weight  $w(\mathbf{x}, \alpha)$  was given by a bell-shaped exponential formula with peak value at zero dip in the common-image gather at  $\mathbf{x}$ .

By means of Laplace’s method and an asymptotic evaluation of the integral (1), Schleicher and Costa (2009) showed that the result of a multipath summation produces a migrated image that is, at each image point  $\mathbf{x}$ , proportional to the migration with stationary velocity value, i.e., the one for which the weight function in integral (1) takes its maximum value, and to the weight factor calculated for this velocity. This analysis implies that the use of a slightly modified weight function,  $\tilde{w}(\mathbf{x}, \alpha) = \alpha w(\mathbf{x}, \alpha)$  provides, at each point  $\mathbf{x}$ , a second migration result that is proportional to the first one, the factor being the stationary value of the velocity at point  $\mathbf{x}$ . Thus, the ratio between the migration results provides this velocity value. This property allows for the determination of a velocity value for all points with a nonzero multi-stack image. A complete velocity model can then be constructed by intelligently filling the gaps and smoothing (Schleicher and Costa, 2009).

### Time-to-depth conversion and velocity estimation

With this procedure, we can automatically construct a time-migration velocity model. However, FWI requires an initial model in depth. Therefore, we need to convert the multi-stack model to depth. For this objective, we chose the time-to-depth conversion of Valente (2013). First performance tests of that conversion procedure were reported in last year’s report by Valente et al. (2014).

The time-to-depth conversion of Valente (2013) is based on the algorithm of the level-set method (see also Santos et al., 2015). It pursues an alternative strategy to perform the time-to-depth conversion. This strategy has the advantage of directly obtaining the velocity field  $v(\mathbf{x})$  and the traveltime  $\tau(\mathbf{x})$ , avoiding to calculate the auxiliary functions  $p(\mathbf{x})$  and  $q(\mathbf{x})$  like in concurrent schemes (Cameron et al., 2007,

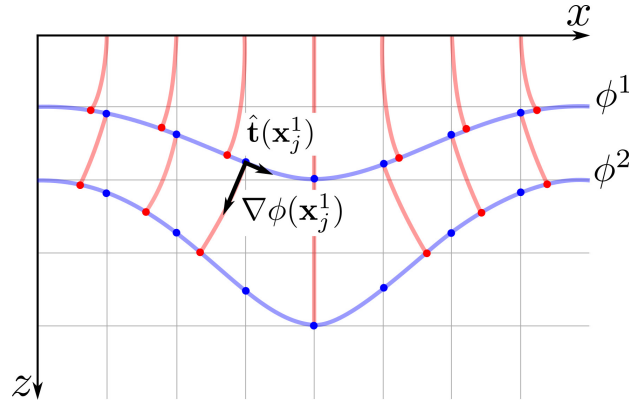


**Figure 1:** Sketch of the image-wavefront propagation algorithm. The ray quantities are not computed where the image-ray paths intersect the desired wavefront (red dots), but rather along vertical lines coincident with the lateral positions of the grid (blue dots). The next step starts from these new base points using tangent vector  $\hat{\mathbf{t}}$  and the travelttime gradient  $\nabla\phi$ .

2008; Iversen and Tygel, 2008). By means of a modified fast-marching conversion algorithm, it directly determines the matrix  $\gamma(\mathbf{x})$  of image-ray emergence points from the already known values of  $v(\mathbf{x})$  and  $\tau(\mathbf{x})$ .

The principal difference to other algorithms is that at every time step, the ray quantities are interpolated at the horizontal coordinates of the given grid, determining the vertical coordinate of the wavefront accordingly (see Figure 1). In this way, it avoids the need to add or remove points on the wavefront or create additional rays. Moreover, since the horizontal dislocations are still small, so are the interpolation errors. In other words, the procedure does not follow individual image rays, but constructs a set of wavefronts for a complete image-ray field by starting with a plane wave at the surface. For the propagation of the image-ray wavefront, it needs only the knowledge of its position at the previous time step. As a consequence of the intermediate horizontal interpolations, this procedure requires the final interpolation of the output quantities in the vertical direction only.

The first step of this algorithm is to propagate the image-wavefront  $\phi(\mathbf{x})$  in the direction of its gradient  $\nabla\phi$ . Points on the new wavefront,  $\phi^{n+1}$ , are obtained from the points on the previous one,  $\phi^n$ , by following segments of image ray (see again Figure 1). The direction of the gradient at each point along the wavefront is perpendicular to the wavefront's tangent vector  $\hat{\mathbf{t}}(x_j)$ . The latter can be approximated by the direction vector to the position of the wavefront at the neighboring grid point. The set of end points of the ray-tracing step (red points in Figure 1) defines the new wavefront  $\phi^{n+1}$ . The second step consists of a linear interpolation to find the points where this new wavefront intersects the vertical grid lines (blue points in Figure 1). In other words, we redefine the calculation points so that they fall exactly on the lateral positions where the wavefront intersects the grid (see Figure 1). In this way, the sampling along the wavefront remains always regular, avoiding the need to add or remove rays. Moreover, this procedure inherently smooths the wavefront so that caustics (which are not allowed for image rays) cannot occur.

At the next time step, the algorithm starts over at the image-ray wavefront at these new coordinates (Figure 1). The depth-converted velocity field at a point  $\mathbf{x} = (x, z)$  is then determined from

$$v(\mathbf{x}) \equiv v^{\text{Dix}}(\gamma = x, \tau(\mathbf{x})). \quad (2)$$

Valente (2013) refer to this wavefront-construction strategy as wavefront propagation, because it does not follow any single image-rays through the model. For further details, see Valente (2013).

### Acoustic full waveform tomography

To test whether the so-obtained depth model has sufficient quality for FWI, we used a modified version of the 2D acoustic time-domain FWT code initially implemented by Kurzmann et al. (2013). Here we briefly summarize the underlying concepts.

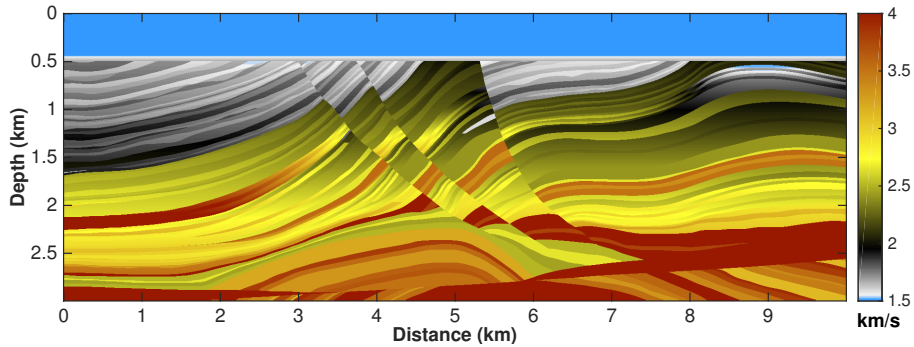


**Figure 2:** True velocity of the modified Marmousi-2 model.

**Forward modeling** The FWT implementation of Kurzmann et al. (2013) solves the homogeneous acoustic wave equation in the time domain by means of a time-domain finite-difference time-stepping method (Alford et al., 1974) with perfectly matched layer (PML) boundary condition (Berenger, 1994; Chew and Weedon, 1994) and massive parallelization comprising domain decomposition (Bohlen, 2002) and shot parallelization (Kurzmann et al., 2009). The distribution of shots on different computers provides a reduction of network traffic and consequently a speedup of the inversion algorithm.

**Inversion** The objective of the code is the reconstruction of an acoustic velocity model. For simplicity, the density is considered constant and not a subject of the inversion. The solution of the inverse problem is based on the time-domain FWT of Tarantola (1984) and Mora (1987a). It comprises the adjoint method and the conjugate gradient method using a least-squares misfit function. For further details, please refer to Kurzmann et al. (2013).

## NUMERICAL EXAMPLE

To test our initial-model construction, we apply it to a modified version of the 2D Marmousi model similar to the one of Kurzmann et al. (2013).

### Model description and acquisition geometry

We modified a section of the Marmousi-2 model (Figure 2) based on Versteeg (1994) and Martin et al. (2002). The velocities are clipped to the range of 1500 to 4000 m/s to reduce computational efforts. The acquisition geometry simulates a marine streamer geometry with length of 5980 m, consisting of 187 shots and a maximum number of 300 receivers per source. Receiver spacing is 20 m and the nearest offset was 45 m. The source time function is a Ricker wavelet with peak frequency  $f_{peak} = 9$  Hz. The model size is  $3 \text{ km} \times 10 \text{ km}$  which, using a grid spacing of 5 m, resulting in a grid size of  $600 \times 2000$  grid points. We set a perfectly matched layer (PML) of 150 m width to avoid artificial boundary reflections in finite-difference modeling. The recording time of the seismic data was 5.6 s with a time discretization of  $7 \cdot 10^{-4}$  s. We chose these parameters to make the conditions for the FWT nearly ideal.

To decrease the computational time for the migration velocity analysis, and to work under more realistic conditions, we resampled the seismic data to 4 ms and windowed the offsets processing only half of them. From these data we extracted a time-migration velocity model using the double multi-stack MVA with velocities between 1400 m/s and 4200 m/s at every 100 m/s. In order to avoid the presence of possible artifacts created during the conversion step, we used strong regularization and smoothed the time-domain model by one pass of a moving average with a  $500 \text{ m} \times 500 \text{ m}$  (100 by 100 points) window. The resulting model is depicted in Figure 3). We then converted this model to depth using image-ray wavefronts as described above.

It is important to note that the time-migration velocity model is less than perfect for a subsequent time migration (see Figure 4). This is to be expected because the central region of the Marmousi model has strong lateral variations for a time migration to work.

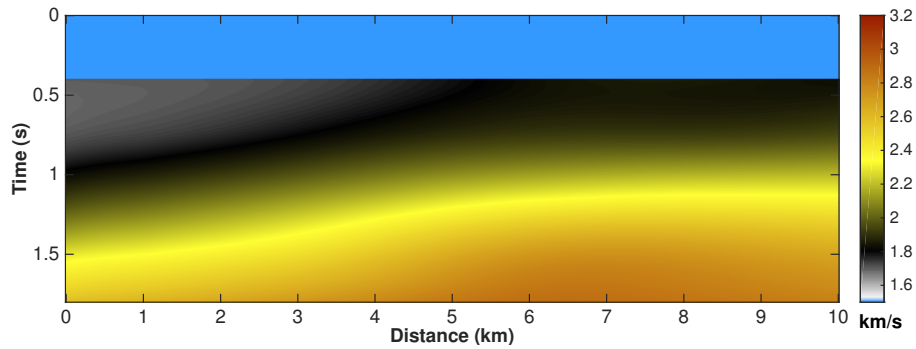


**Figure 3:** Time-migration velocity model obtained by the multi-stack MVA with strong regularization.

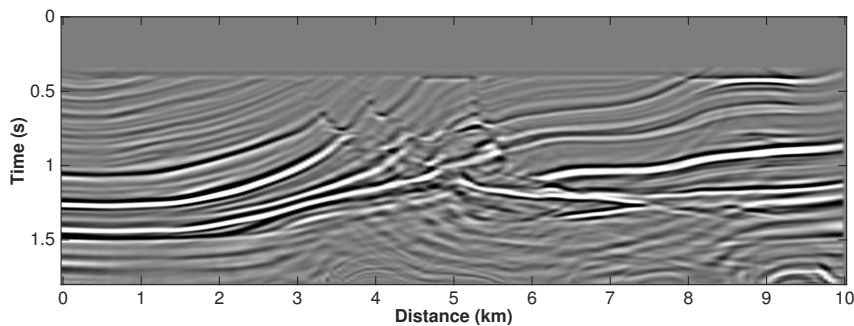


**Figure 4:** Time migrated image with the model obtained by the multi-stack MVA with strong regularization.

### Initial velocity models

For our evaluation we compare the results of FWT with four initial velocity models (see Figure 5):

1. **Smoothed velocity model:** smooth initial velocity model (Figure 5(a)), generated by application of a 2D Gaussian filter (size  $1250 \text{ m} \times 1250 \text{ m}$ ,  $\sigma=51$ ) to the sub-seafloor area of the true velocity model (Figure 2). This is the same P-wave velocity model used by Kurzmann et al. (2013) in their sensitivity analysis of attenuation.
2. **Homogeneous velocity model:** a constant velocity model of 3 km/s (Figure 5(b)).
3. **Vertical gradient velocity model:** this models ranges from 1.6 km/s on the upper part to 4 km/s on the bottom (Figure 5(c)).
4. **Estimated velocity model:** time-migration velocity model from the double multi-stack MVA (Figure 3) converted to depth using image-ray wavefronts as described above. To decrease the computational time, we resampled the seismic data to 4 ms and windowed the offsets processing only half of them. In order to avoid the presence of possible artifacts created during the conversion step, we smoothed the time-domain model by one pass of a moving average with a  $500 \text{ m} \times 500 \text{ m}$  (100 by 100 points) window. The so-obtained model is depicted in Figure 5(d).

### Practical aspects and inversion workflow

Like Kurzmann et al. (2013), we used 32 shots to perform the inversion. Also, we set up a specific five-step workflow with parameters summarized in Table 1.

The first column of the table presents the minimum number of iterations for each step. The threshold in the second column represents the stop criterion. If the relative change between the data misfit in three

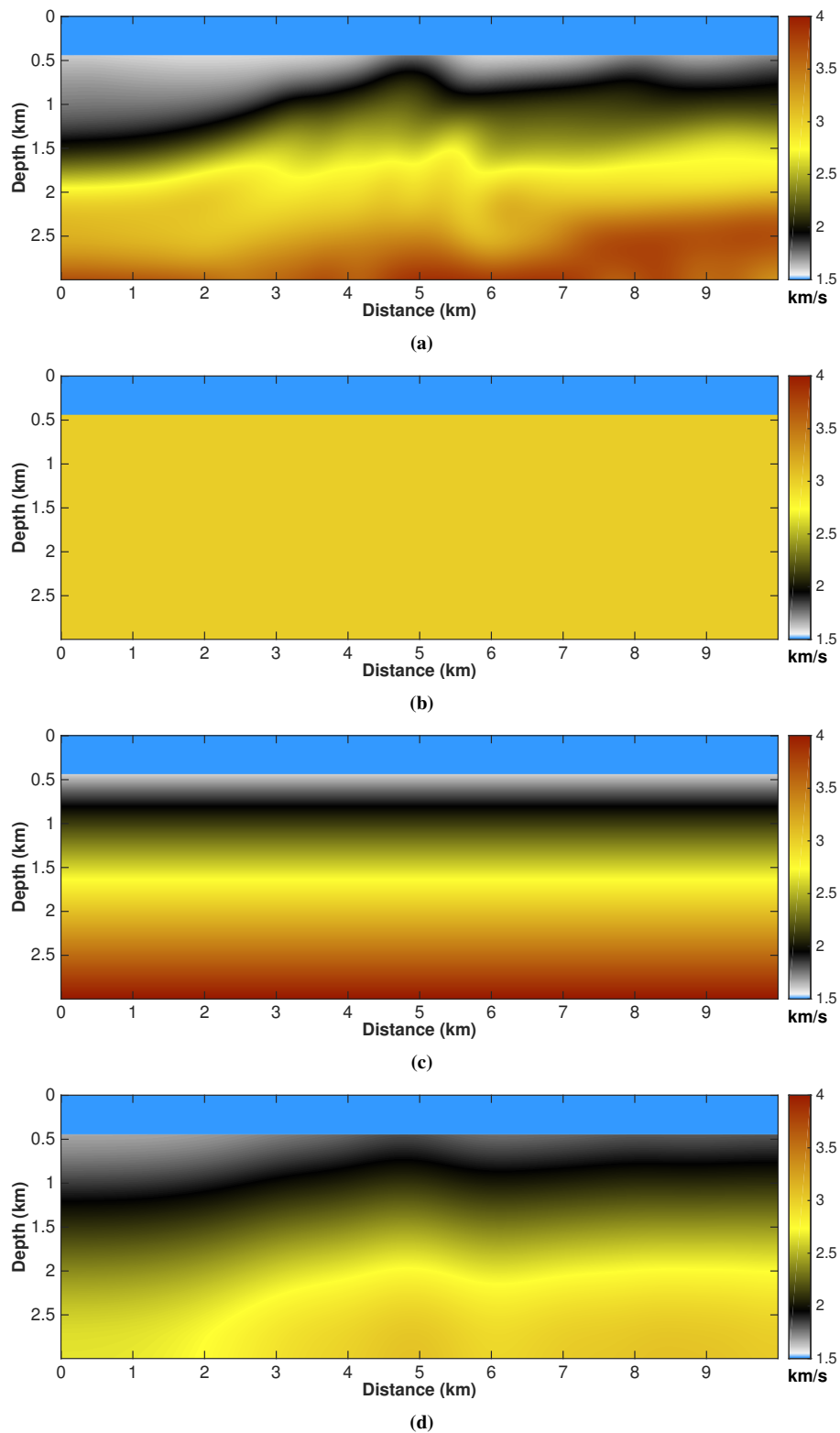


**Figure 5:** Initial models: (a) smoothed version obtained after low-pass filtering of the true model (Figure 2); (b) homogeneous velocity model ( $v = 3 \text{ km/s}$ ); (c) constant vertical gradient; (d) velocity model obtained by the double multi-stack MVA converted from time-to-depth using the image-wavefront propagation.

**Table 1:** Time-domain FWI workflow

Number of iterations	Threshold	Time-domain filter frequencies			
		F1	F2	F3	F4
15	0.005	0	0	0.5	4
15	0.005	0	0	1	6
15	0.005	0	0	3	9
15	0.005	0	0	5	15
200	0.005	-	-	-	-

subsequent iterations (after the minimum number of iterations) does not exceed the threshold, the algorithm proceeds to the next step.

Finally, the last four columns of Table 1 indicate the corner frequencies for the band-pass filters used in each step (linear increase from zero to one between  $F1$  and  $F2$ , one between  $F2$  and  $F3$ , linear decrease from one to zero between  $F3$  and  $F4$ ). In this case, we used only low-pass filters ( $F1 = F2 = 0$  for all steps). The frequency range increased from step to step until, in the last step, the full frequency content of the data was used.

## Results

We then executed the FWT code on the original undecimated (i.e., almost ideal) data using the four starting models of Figure 5. For better evaluation, we saved intermediate FWT processing results after 100 and 200 iterations of the inversion process. Figures 6 and 7 depict the recovered velocity models and their differences to the true one after 100 iterations, and Figures 8 and 9 show the corresponding results after 200 iterations. We see that the results using the depth-converted multi-stack model are comparable in quality to the ones obtained with the smoothed model or the true vertical gradient and clearly superior to the ones obtained with the constant starting model.

The final inverted models, after the FWT code reached convergence at the end of the workflow, are shown in Figure 10 and their differences to the true one in Figure 11. Except for the boundary region, the model inverted starting at the converted time model reaches the same quality as the one obtained from the smoothed model and is, at some places, even superior to the one obtained from the true vertical gradient.

## CONCLUSION

In this work we have presented a workflow for the construction of initial velocity-models for FWT methods. In an attempt to aid the search for more efficient model-building tools, we investigate the applicability of a recent automatic time MVA method. This method stacks twice over migrated images for many models with different weights in order to extract stationary migration velocities from the ratio of the images. Thus, it is able to generate a velocity model and a time-migrated image without a priori information.

For the use of such a velocity model in FWT methods, the result needs to be converted from time to depth. For this purpose, we chose a strategy based only on image-ray wavefront propagation. The results confirmed the method's efficiency in very complex geology structures, i.e., models with strong velocity variations.

Our first numerical results indicate the potential of using a combination of these methods to achieve a fully automatic tool for initial-model building in a FWT workflow. In our tests, the method was able to produce a sufficiently accurate initial model for an FWT under nearly ideal conditions converge to a model of comparable quality as when starting at a smoothed version of the true model. This indicates that correct background velocity information can be successfully extracted from automatic time-domain migration velocity analysis even in media where time-migration cannot provide satisfactory seismic images.

Future investigations will have to show whether some model detail can be already introduced in the time domain or added in an additional depth-domain MVA step in order to reduce the number of necessary FWT iterations, and if the inversion can still be successful from such initial models if the data are less than ideal.

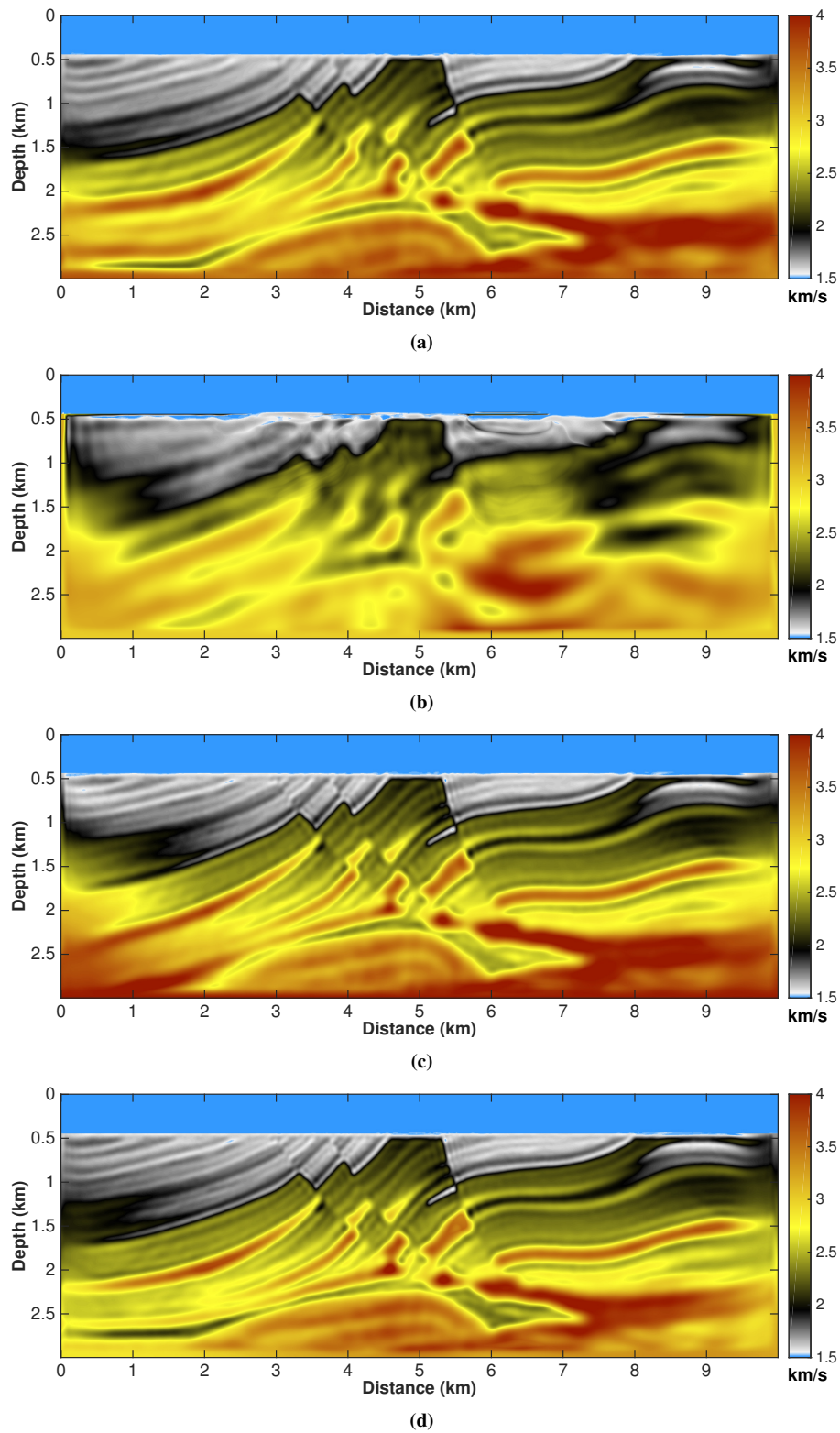


**Figure 6:** (a) to (d) show the recovered velocity models after 100 iterations for the acoustic FWI starting with the velocity model in Figure 5.

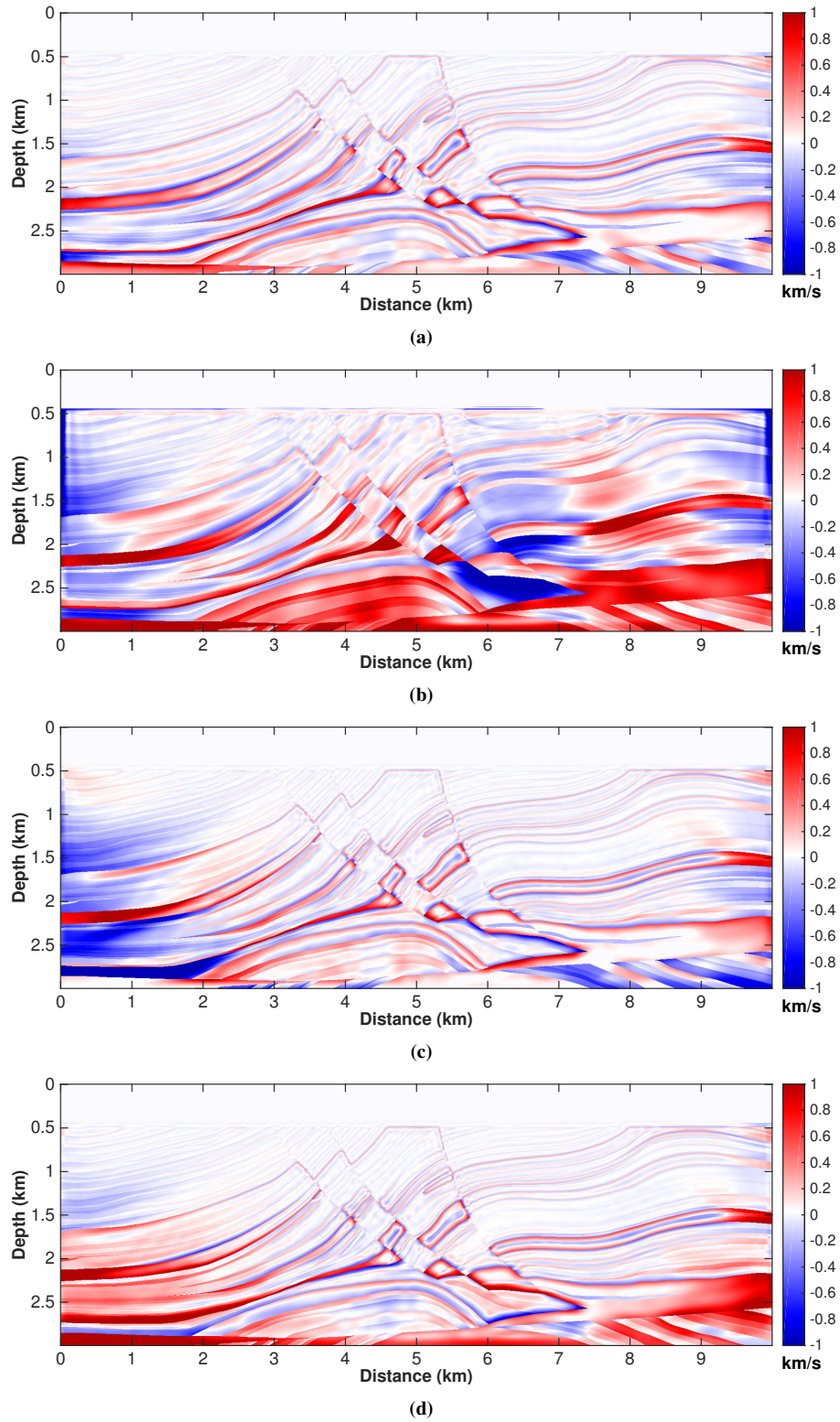


**Figure 7:** (a) to (d) show the difference of the results in Figure 6 with respect to the true model in Figure 2.

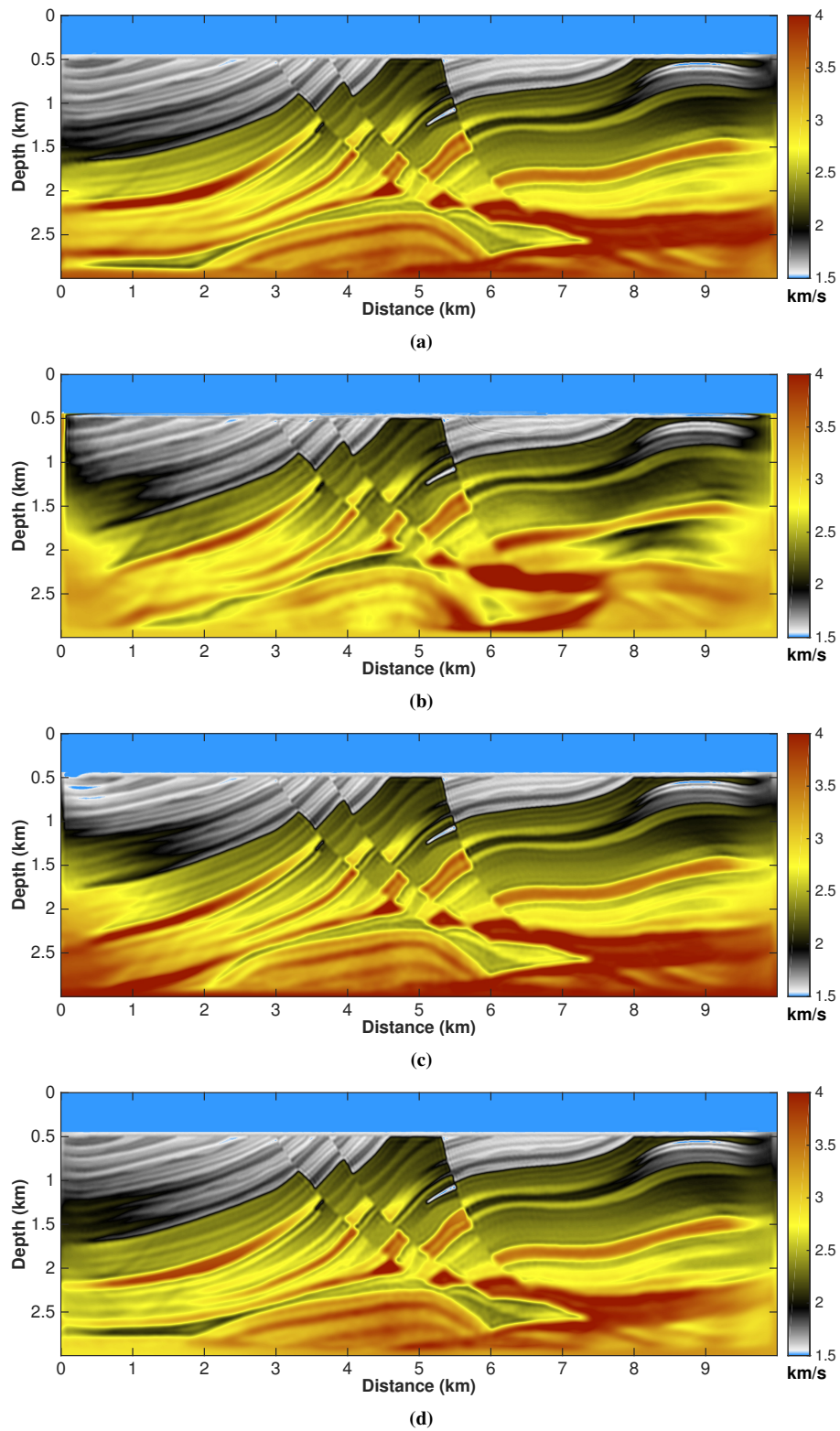


**Figure 8:** (a) to (d) show the recovered velocity models after 200 iterations for the acoustic FWI starting with the velocity model in Figure 5.

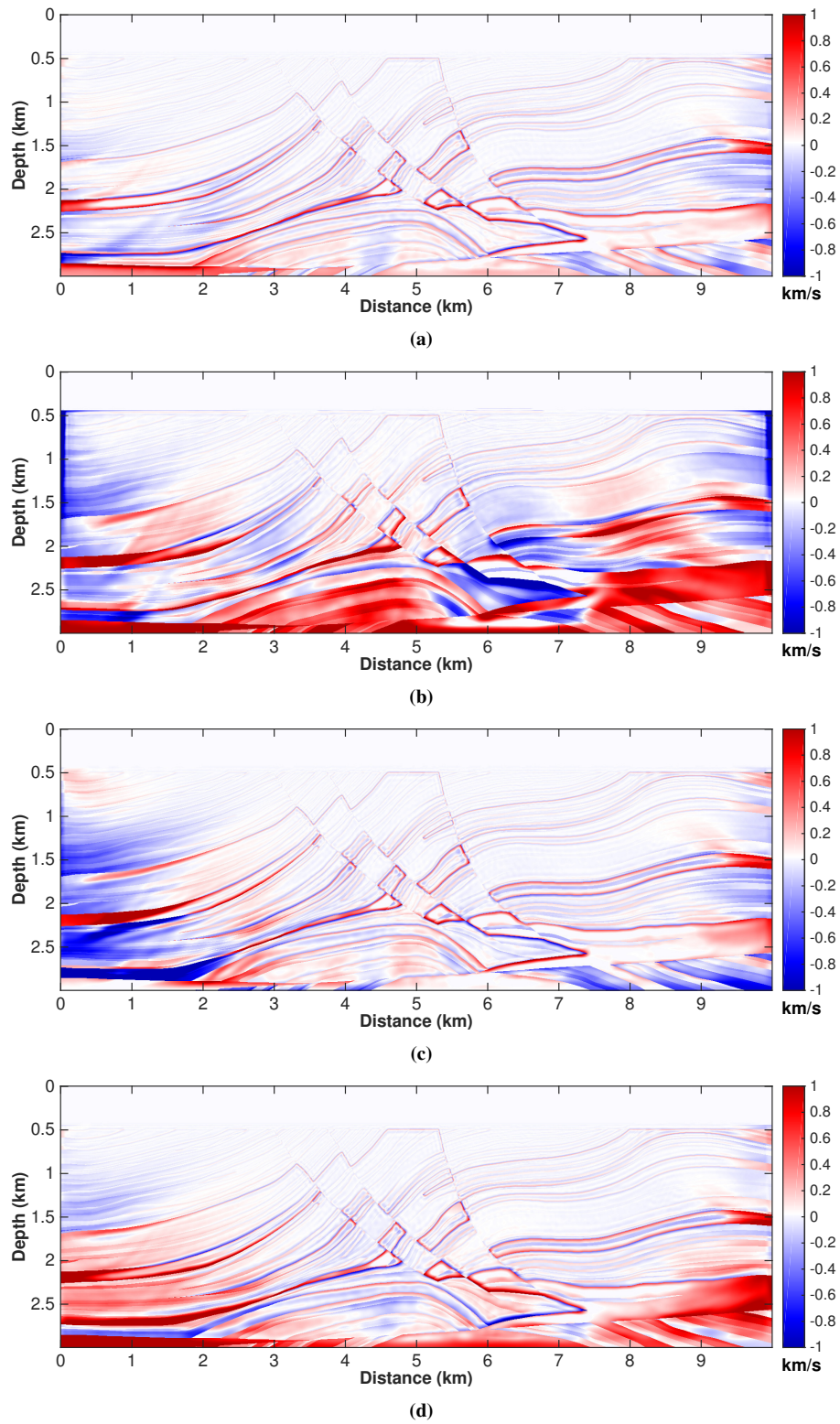


**Figure 9:** (a) to (d) show the difference of the results in Figure 8 with respect to the true model in Figure 2.

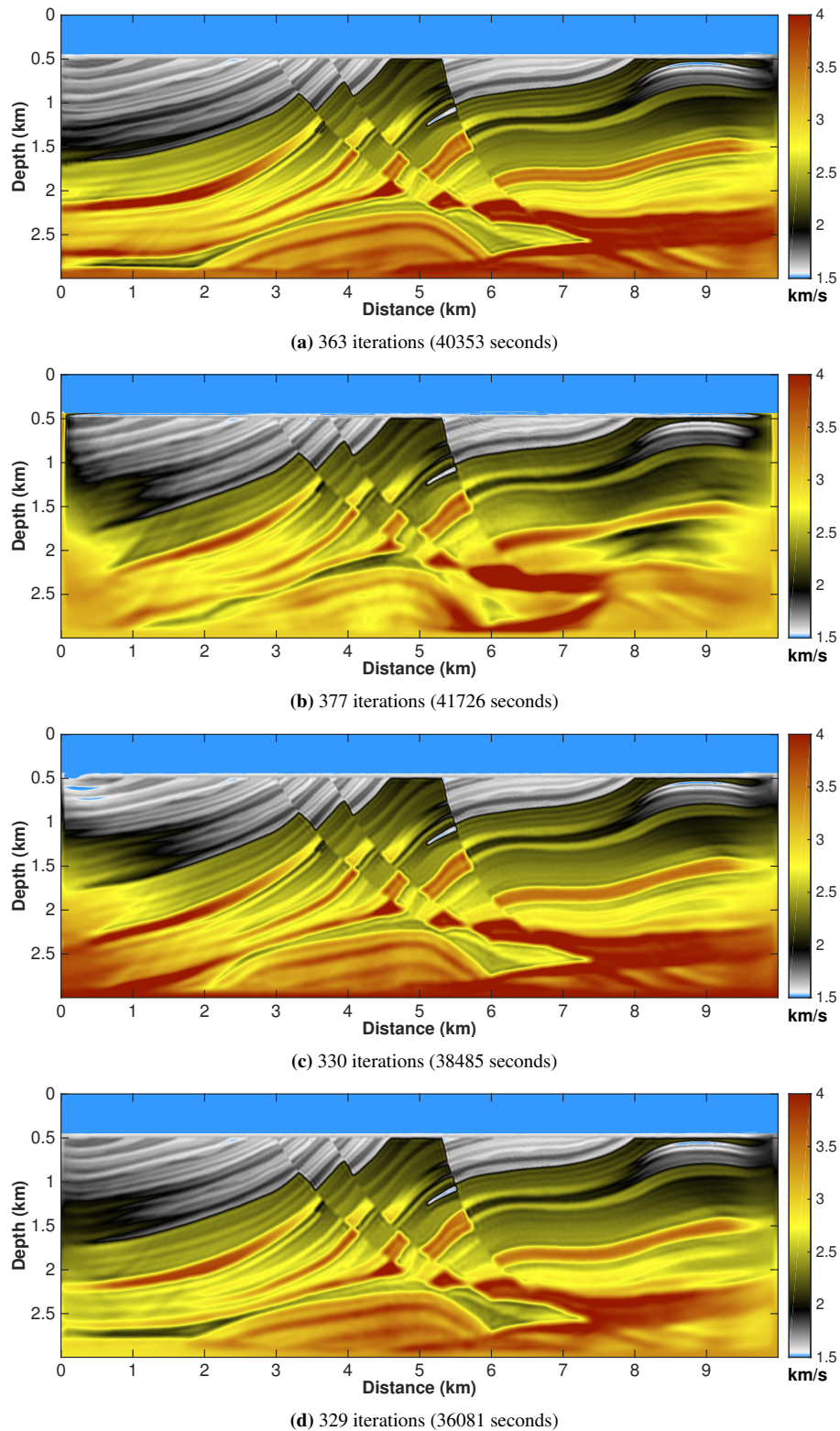


**Figure 10:** (a) to (d) show the recovered velocity models when they complete the inversion workflow for the acoustic FWI starting with the velocity model in Figure 5. The individual amount of required iterations differs from each other.

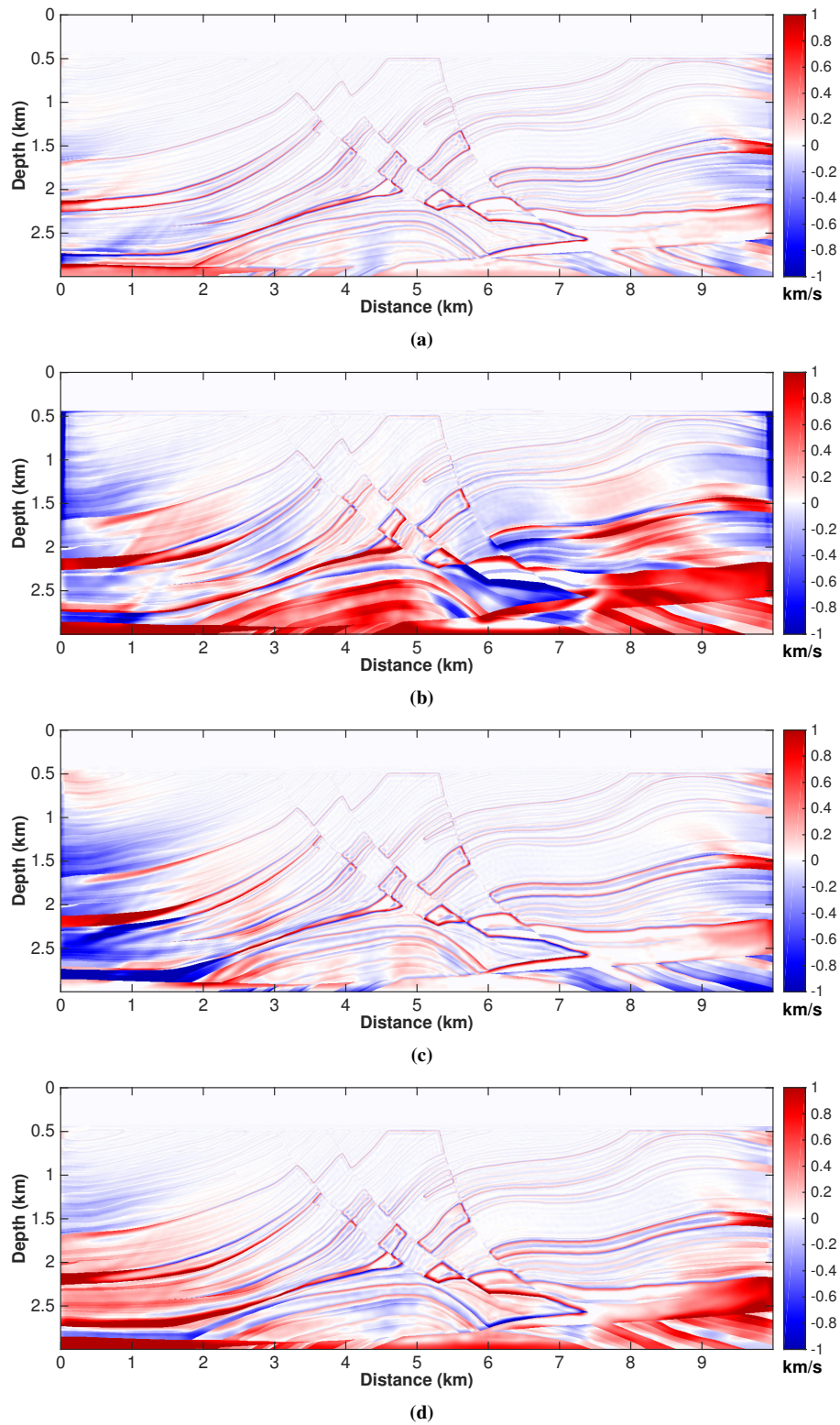


**Figure 11:** (a) to (d) show the difference of the results in Figure 10 with respect to the true model in Figure 2.

## ACKNOWLEDGMENTS

This work was kindly supported by the sponsors of the *Wave Inversion Technology (WIT) Consortium*. We acknowledge Petrobras and CGG as well as the Brazilian national research agencies CNPq, FAPESP, and CAPES. Henrique B. Santos thanks CGG-Brazil and Petrobras for his fellowships. Furthermore, we are grateful for using the supercomputers JUROPA at Jülich Supercomputing Centre and ForHLR at Steinbuch Centre for Computing (KIT, Karlsruhe; funded by the state of Baden-Württemberg and the federal government of Germany).

## REFERENCES

- Alford, R. M., Kelly, K. R., and Boore, D. M. (1974). Accuracy of finite-difference modeling of the acoustic wave equation. *Geophysics*, 39(6):834–842.
- Berenger, J. P. (1994). A Perfectly Matched Layer for the Absorption of Electromagnetic Waves. *Journal of Computational Physics*, 114:185–200.
- Biondi, B. and Almomin, A. (2014). Simultaneous inversion of full data bandwidth by tomographic full-waveform inversion. *Geophysics*, 79(3):WA129–WA140.
- Bohlen, T. (2002). Parallel 3D viscoelastic finite difference seismic modelling. *Computers and Geosciences*, 28:887–899.
- Cameron, M. K., Fomel, S. B., and Sethian, J. A. (2007). Seismic velocity estimation from time migration. *Inverse Problems*, 23:1329–1369.
- Cameron, M. K., Fomel, S. B., and Sethian, J. A. (2008). Time-to-depth conversion and seismic velocity estimation using time-migration velocity. *Geophysics*, 73(5):VE205–VE210.
- Chew, W. C. and Weedon, W. H. (1994). A 3D perfectly matched medium from modified Maxwell's equations with stretched coordinates. *Microwave and Optical Technical Letters*, 7(13):599–604.
- Fichtner, A., Kennett, B. L. N., Igel, H., and Bunge, H.-P. (2009). Full seismic waveform tomography for upper-mantle structure in the Australasian region using adjoint methods. *Geophysical Journal International*, 179(3):1703–1725.
- Iversen, E. and Tygel, M. (2008). Image-ray tracing for joint 3D seismic velocity estimation and time-to-depth conversion. *Geophysics*, 73(3):S99–S114.
- Kurzmann, A., Köhn, D., Przebindowska, A., Nguyen, N., and Bohlen, T. (2009). 2D Acoustic Full Waveform Tomography: Performance and Optimization. In *Extended Abstracts, 71st Conference and Technical Exhibition*. EAGE.
- Kurzmann, A., Przebindowska, A., Köhn, D., and Bohlen, T. (2013). Acoustic full waveform tomography in the presence of attenuation: a sensitivity analysis. *Geophysical Journal International*, 195(2):985–1000.
- Landa, E., Fomel, S., and Moser, T. J. (2006). Path-integral seismic imaging. *Geophysical Prospecting*, 54(5):491–503.
- Martin, G. S., Marfurt, K. J., and Larsen, S. (2002). Marmousi-2: An updated model for the investigation of AVO in structurally complex areas. In *SEG Technical Program Expanded Abstracts, 72 Annual International Meeting*, pages 1979–1982. SEG.
- Mora, P. (1987a). Elastic inversion of field data. *SEP report*, 51:211–218.
- Mora, P. (1987b). Nonlinear two-dimensional elastic inversion of multioffset seismic data. *Geophysics*, 52(9):1211–1228.
- Mora, P. (1989). Inversion = migration + tomography. *Geophysics*, 54(12):1575–1586.

- Pratt, R. G. (1990). Inverse theory applied to multi-source cross-hole tomography. Part 2: elastic wave-equation method. *Geophysical Prospecting*, 38:311–329.
- Pratt, R. G. (1999). Seismic waveform inversion in the frequency domain, Part 1: Theory and verification in a physical scale model. *Geophysics*, 64(3):888–901.
- Pratt, R. G. and Worthington, M. H. (1990). Inverse theory applied to multi-source cross-hole tomography. Part 1: acoustic wave-equation method. *Geophysical Prospecting*, 38:287–310.
- Prieux, V., Lambaré, G., Operto, S., and Virieux, J. (2012). Building starting models for full waveform inversion from wide-aperture data by stereotomography. *Geophysical Prospecting*, 61:109–137.
- Santos, H. B., Valente, L. S. S., Costa, J. C., and Schleicher, J. (2015). Time-to-depth conversion and velocity estimation by wavefront-propagation. In *SEG International Exposition and 85th Annual Meeting*, New Orleans, Louisiana. Society of Exploration Geophysicists.
- Schleicher, J. and Costa, J. C. (2009). Migration velocity analysis by double path-integral migration. *Geophysics*, 74(6):WCA225–WCA231.
- Symes, W. W. (2008). Migration velocity analysis and waveform inversion. *Geophysical Prospecting*, 56(6):765–790.
- Tarantola, A. (1984). Inversion of seismic reflection data in the acoustic approximation. *Geophysics*, 49(8):1259–1266.
- Tarantola, A. (1986). A strategy for nonlinear elastic inversion of seismic reflection data. *Geophysics*, 51(10):1893–1903.
- Valente, L. S. S. (2013). Evaluation of algorithms for the conversion of velocity models from time to depth. Master's thesis, Federal University of Pará. In Portuguese.
- Valente, L. S. S., Santos, H. B., Costa, J. C., and Schleicher, J. (2014). A strategy for time-to-depth conversion and velocity estimation. *Annual WIT Report*, 18:137–151.
- Versteeg, R. (1994). The Marmousi experience: Velocity model determination on a synthetic complex data set. *The Leading Edge*, 13:927–936.
- Yang, P., Gao, J., and Wang, B. (2015). A graphics processing unit implementation of time-domain full-waveform inversion. *Geophysics*, 80(3):F31–F39.